Journal of Materials Chemistry C

ROYAL SOCIETY OF CHEMISTRY

PAPER

View Article Online
View Journal

Cite this: DOI: 10.1039/d0tc03008b

Novel electrochemical devices with high contrast ratios and simultaneous electrochromic and electrofluorochromic response capability behaviours†

Hsiang-Ting Lin,‡[a] Jung-Tsu Wu,‡[a] Mu-Huai Chen[a] and Guey-Sheng Liou *[ab]

Received 25th June 2020,
Accepted 13th August 2020

DOI: 10.1039/d0tc03008b

rsc.li/materials-c

In this work, we studied the novel redox-active material *N*,*N*,*N*′,*N*′-tetrakis(4-methoxyphenyl)-1,1′-biphenyl-4,4′-diamine (**TPB**) and found it to exhibit the crucial optical characteristics of high PL quantum yields both in solution (Φ_{PL} = 34.5%) and solid (Φ_{PL} = 32.4%) states. This unique PL characteristic was key for fabricating liquid-type and gel-type electrochemical devices displaying high-performance electrochromic (EC) and electrofluorochromic (EFC) behaviours at the same time. All of the obtained devices based on **TPB** exhibited excellent EFC performance, including rapid switching response times, unprecedented PL intensity contrast ratio (I_{off}/I_{on}) values of up to 374 (the highest value reported to the best of our knowledge), and remarkable levels of electrochemical stability. In addition, these devices could, without UV irradiation, be transformed between being highly transparent and colourless devices and being truly black ones through switching between their original and oxidative states.

Introduction

The cathode ray tube (CRT) played an important role in displays for several decades from the 1920s until it was replaced by plasma, liquid crystal display (LCD), and other solid-state devices such as light-emitting diodes (LEDs) and organic light-emitting diodes (OLEDs).[1–3] However, consumers are still not satisfied with the performances of these devices, so displays with more vivid, colourful and short response times are being pursued. Based on the demands of the market, ''flexibility and transparency'' are goals of industry pursuing next-generation displays.

Transparent displays act in the absence of applied power just like glass with high transparency, while in the working state they show high resolution and contrast. These features make them attractive for applications in electronic devices, such as smart glasses (Google Glass), wearable devices and head-up displays. These applications are anticipated to bring about a huge commercial opportunity. While transparent display technology has already been commercialized, poor contrast remains a crucial obstacle to further commercialization and still needs to be contended with.[4,5]

Electrochromic (EC) materials among other materials have been used to fabricate panchromatic shutters for enhancing the image contrast of transparent displays. Reynolds and co-workers published their work on developing the first display that could be switched between black and transparent with EC materials in 2008.[6] Nevertheless, EC materials with high contrast (ΔL^*) in CIE $L^*a^*b^*$ coordinates were difficult to obtain, especially for devices that could be switched from a colourless and transparent neutral form to a truly black oxidized form.[7–12] We have recently developed a series of novel redox-active triphenylamine (TPA)-based polymers and small-molecule materials that could be used to fabricate highly transparent to truly black EC devices (ECDs) as panchromatic shutters of transparent displays.[13–15] The photo- and electro-active behaviours of TPA derivatives have been studied intensively, and they have been shown to effectively stabilize the resulting radical cations after oxidation and exhibit a noticeable change of coloration during the oxidation redox process. Therefore, numerous TPA-based derivatives and polymers have been reported for EC applications. Of them, the *N*,*N*,*N*′,*N*′-tetrakis(4-methoxyphenyl)-*p*-phenylene-diamine (**TPPA**)/*N*,*N*,*N*′,*N*′-tetrakis(4-methoxyphenyl)-1,1′-biphenyl-4,4′-diamine (**TPB**)/heptyl viologen tetrafluoroborate (**HV**) system has been shown to display a particularly high contrast (ΔL^*) between highly transparent (L^* = 91.92; a^* = −6.02; b^* = 5.13) at the neutral state and truly black (L^* = 5.50; a^* = 0.87; b^* = −0.03) at the oxidized state during the

[a] Institute of Polymer Science and Engineering, National Taiwan University, 10607, Taipei, Taiwan. E-mail: gsliou@ntu.edu.tw
[b] Advanced Research Center for Green Materials Science and Technology, National Taiwan University, 10607, Taipei, Taiwan

† Electronic supplementary information (ESI) available. CCDC 1988872. For ESI and crystallographic data in CIF or other electronic format see DOI: 10.1039/d0tc03008b

‡ These authors equally contributed to this work.

oxidation redox process.[15] Surprisingly, we noticed unique optical characteristics for compound **TPB**, having observed it exhibiting good photoluminescence (PL) characteristics both in solution and solid states.[16] With excellent PL and EC features, **TPB** was thus expected to be a promising candidate as an electrofluorochromic (EFC) material. Most EFC materials with high PL contrast have to date been reported based on polymers,[17–24] small molecules,[25–30] and metallo-supramolecular polymers,[31–33] respectively. But there have been few reports of EFC materials based on panchromatic black shutters. Even though Joseph and co-workers reported an EFC device (EFCD) that could exhibit EC switching from a transparent yellow neutral state (L^* = 97, a^* = −5, b^* = 16) to black oxidized state (L^* = 41, a^* = 2, b^* = 8),[34] the development of an advanced and ideal EFCD with a high EC contrast ratio from a highly transparent and colourless neutral state to a panchromatic black oxidized state is still an ongoing issue.

In the work described in this article, we developed two types of liquid-type EFCDs displaying high PL contrast ratio (I_{off}/I_{on}) values, with one type based on **TPPA**/**TPB**/**HV** and the other based on **TPB**/**HV**. Furthermore, a highly transparent gel-type EFCD derived from **TPB**/**HV** was also fabricated to investigate the EFC performance. We expect this facile and judicious approach to find use as a new step for both EC and EFCD applications.

Experimental section

Fabrication of the EFCD

To make the blank devices, first a thermoset adhesive was dispensed onto a 20 mm × 20 mm square shape of a blank ITO-glass (5 Ω sq^{-1}) using a fully-automatic dispenser, and a tiny hole was retained. Another blank ITO-glass was pasted onto this composite and then baked at 150 °C for two hours. The gap between these two ITO-glasses was controlled by dispersing glass balls with an average grain size of about 120 μm into the adhesive. Two different kinds of transparent electrolyte with related redox-active materials were injected into the device by using a vacuum encapsulating system, and then the tiny hole was sealed with UV adhesive. Solution-type electrolyte devices were derived from a mixture of propylene carbonate (PC) and a γ-butyrolactone (GBL) solution, while gel-type electrolyte devices were fabricated from a polymer solution containing 5.6 mg of **poly(4MMA–1HEMA)**, 0.4 mg of Desmodur® N3200, 0.07 mg of dibutyltin diacetate and 0.05 mL of GBL. The gel-type polymer electrolyte was cured at 75 °C for 2 hours.

Materials

TPPA and **TPB** were synthesized according to the previously reported method.[15] A single crystal of **TPB** was obtained by recrystallizing the **TPB** in hexane and toluene. A solution of copolymer of poly(4MMA–1HEMA) with a 4 : 1 molar ratio of methyl methacrylate (MMA) to 2-hydroxyethyl methacrylate (HEMA) was obtained by combining MMA, HEMA and 2,2′-azobis(2-methylpropionitrile) (AIBN) in PC and stirring the resulting mixture at 75 °C for 24 hours as described in ESI.† HV was acquired by first dissolving 4,4′-bipyridine and excess 1-bromoheptane in acetonitrile, and refluxing this solution for 6 hours; then filtration of this solution was carried out followed by dissolving the filtered part in DI water, to which excess saturated sodium tetrafluoroborate aqueous solution was then added to produce crude precipitate that was collected and recrystallized using ethyl acetate. The rest of the chemicals were purchased from a commercial source and used as received.

Measurements

Electrochemical measurements were taken with a CH Instrument 611B electrochemical analyzer or CH Instrument 612C electrochemical analyzer. Ultraviolet-visible (UV-vis) spectra were acquired by using an Agilent 8453 UV-visible spectroscopy system. CIELAB data were collected from a JASCO V-650 UV-vis spectrophotometer. Cyclic voltammetry was conducted by using two-electrode devices, each with a 20 mm × 20 mm working area and gap of 120 μm, at a scan rate of 50 mV s^{-1}. Spectro-electrochemical and EC properties were assessed by combining the results obtained using a CH Instrument 612C electrochemical analyzer and Agilent 8453 UV-visible spectroscopy system in the wavelength range 300 and 1100 nm. PL spectra were acquired using a Fluorolog-3 spectrofluorometer. The relative PL quantum yield (Φ_{PL}) values of the samples in solution state were measured by using quinine sulfate dissolved in 1 N sulfuric acid as a reference standard (Φ_{PL} = 0.546), and the Φ_{PL} of the powder form was determined by using a calibrated integrating sphere.

Results and discussion

Optical properties resulting from TPB and TPPA

The optical properties of **TPB** and **TPPA** are depicted in Fig. 1 and Fig. S1, Table S1 (ESI†). The absorption maximums (λ_{abs}) of **TPB** were observed to be located at 351 and 362 nm in solution and solid states, and these materials exhibited strong cyan-blue emissions under UV-irradiation with quantum yields of 34.5% and 32.4%, respectively. To comprehend the unique optical behaviour in depth, the geometric structure and packing arrangement of **TPB** in a single crystal were obtained as shown

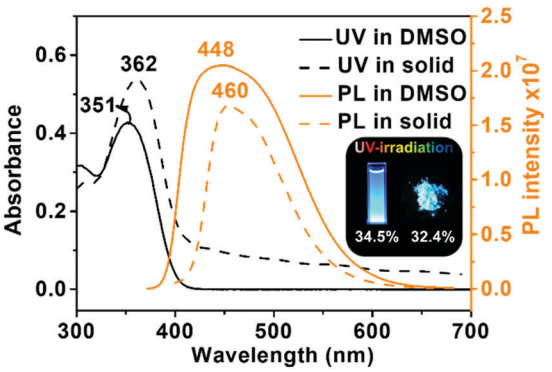

Fig. 1 Absorption and PL spectra of **TPB** in DMSO solution and solid states. (Solution concentration: 10 μM).

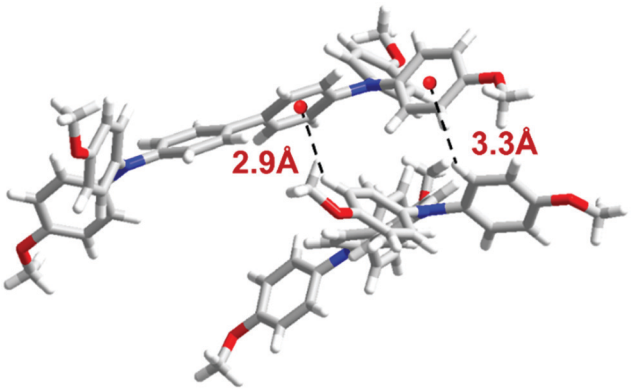

Fig. 2 A perspective view of the packing arrangement of **TPB**.

in Fig. 2 and Table S2 (ESI†). The results revealed that the C–H···π hydrogen bonds with lengths of 2.9 Å and 3.3 Å formed between the protons of **TPB** and the π electron cloud of the phenyl ring from the neighbouring molecular chain. These C–H···π hydrogen bonds locked the intermolecular motion and suppressed π–π stacking effectively, leading to a strong emission of **TPB** in the solid state. PL spectra of **TPB** dissolved in various solvents of different DMSO/water fractions were also acquired (Fig. S2, ESI†), and analysis of these spectra confirmed the special PL behaviour. In addition, cyclic voltammetric (CV) diagrams and UV absorption spectra of TPPA and **TPB** in acetonitrile were obtained, and are illustrated in Fig. S3 (ESI†). Energy levels were calculated from these data and are summarized in Table S3 (ESI†).

EFC properties of liquid-type EFCDs

The liquid-type EFCD derived from a combination of 0.5 μmol **TPPA**, 1.5 μmol **TPB** and 2.0 μmol **HV** without additional supporting electrolyte was used to investigate the fluorescence intensity changes at different applied potentials as shown in Fig. 3a and b. This EFCD emitted strong blue light under UV irradiation with a PL emission maximum wavelength (λ_{em}) of 449 nm. According to our previous work, when the applied voltage was increased from 0.0 to 1.2 V, the device displayed full absorption over the visible light region. Hence, the PL intensity of the **TPPA/TPB/HV** device was almost extinguished with a high PL contrast ratio (I_{off}/I_{on}) of 374, a value higher than that of the previous work (337).[24] The original intensity of the emitted light for the device was again quickly and fully realized when the applied voltage was removed. These PL switching behaviours are illustrated in Fig. 3c and d, and the device needed only 3.7 and 6.9 seconds for achieving at least 90% turn-on and turn-off, respectively. Such a rapid response allowed the system to display an outstanding PL contrast ratio (I_{off}/I_{on}) of 341 even under rapid switching (20 seconds per cycle). Consequently, the **TPPA/TPB/HV** devices showed excellent performance in several regards, including excellent EC behaviour from colourless to panchromatic absorption over the visible light region and EFC characteristics with high PL contrast ratio and quick response switching, implying its great

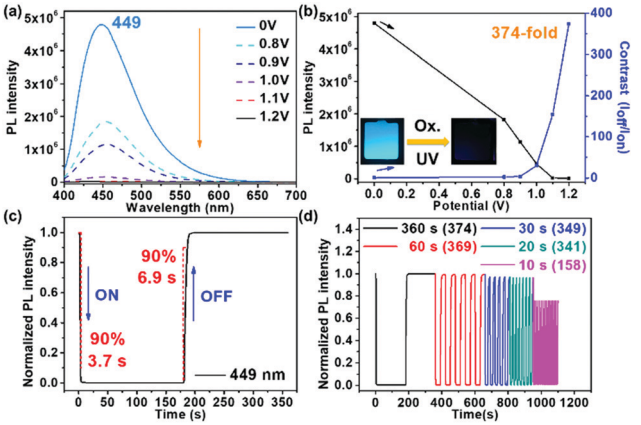

Fig. 3 (a) PL spectra, (b) plots of PL and contrast *vs.* potential, (c) fluorescence switching responses, and (d) switching time testing of liquid-type EFCDs based on **TPPA/TPB/HV**. The switching time testing involved taking measurements at different step cycle times of 360, 60, 30, 20, and 10 s, respectively, by applying voltages between −0.1 and 1.2 V. The devices, each with a gap of 120 μm, were derived from ITO glass with a 2 cm × 2 cm active area.

potential for remarkably effective use in dual functional optoelectronic displays.

Afterwards, we set out to determine whether we could retain the excellent performance of these EFCDs while reducing their cost, specifically by removing the 0.5 μmol **TPPA** and 0.5 μmol of the **HV** from the liquid-type EFCDs to obtain a **TPB/HV** system. As shown in Fig. 4a and b, the PL contrast ratio still remained at a high value, specifically at 336. The fluorescence switching characteristics were also assessed as shown in Fig. 4c and d. The response times for both turn-on and turn-off processes could be reduced to 1.9 and 5.8 seconds, respectively. This improvement led to an enhanced contrast ratio at the shorter switching cycle (293 for just 10 seconds per cycle).

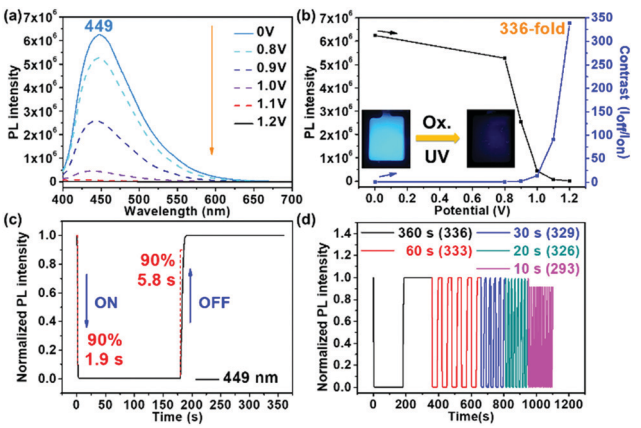

Fig. 4 (a) PL spectra, (b) plots of PL and contrast *vs.* potential, (c) fluorescence switching responses, and (d) switching time testing of liquid-type EFCDs based on **TPB/HV**. The switching time testing involved taking measurements at different step cycle times of 360, 60, 30, 20, and 10 s, respectively, by applying voltages between −0.1 and 1.2 V. The devices, each with a gap of 120 μm, were derived from ITO glass with a 2 cm × 2 cm active area.

Based on the performance and cost considerations, the device derived from the **TPB/HV** system was considered to be a favourable and reasonable option for practical applications.

EFC properties of gel-type EFCDs

Not only the high performance but also the safety of devices is an important issue of concern. Using a gel-type supporting electrolyte is a common approach to avoid splashes when accidents happen, but do cause some deficiencies such as longer response times, higher working voltages and lower contrast ratios. To address this dilemma and improve the EFCD performance simultaneously, poly(MMA–HMEA)s with different molar ratios of MMA to HMEA were synthesized. Here a molar ratio of 4 : 1 was found to be suitable, and was used in gel-type electrolyte EFCDs successfully. The details of the processes used to fabricate the gel-type devices are described in ESI† and depicted in Fig. 5 and Fig. S4, S5 (ESI†).

The EFC behaviours of gel-type EFCD containing 1.5 μmol **TPB** and 1.5 μmol **HV** without supporting electrolyte was investigated as depicted in Fig. 6. While the PL performances of the gel-type devices were slightly inferior to those of the corresponding liquid-type devices, the unique optical properties of **TPB** still resulted in outstanding EFC performance, such as a PL switching contrast ratio as high as 240 and short switching times of 2.7 and 7.5 seconds for turn-on and turn-off processes, respectively.

Another merit of this approach involving the deployment of the **TPB/HV** systems was found to be the resulting remarkable electrochemical stability, as illustrated in Fig. 7 and Fig. S6 (ESI†). After 1000 cycles of on–off switching for both liquid-type devices, and 500 cycles for the gel-type **TPB/HV** EFCDs, these two systems demonstrated excellent electrochemical stability with the reversibility levels of up to 99%.

EC properties of EFCDs

The EC behaviours of liquid-type **TPPA/TPB/HV** devices had already been reported previously.[15] Therefore, we only focused on the **TPB/HV** devices with the two different types electrolyte systems. As shown in Fig. 8a, the CV diagrams of the liquid- and gel-type devices showed negligible differences of oxidative potentials, implying that the difference between types of electrolyte used was not the issue affecting the working voltage in this study. Upon oxidation, the characteristic absorption bands at wavelengths of about 479, 606 and 669 nm increased in intensity, and only less than 9% of the visible light in the range 400 to 700 nm could pass through the device, as illustrated in

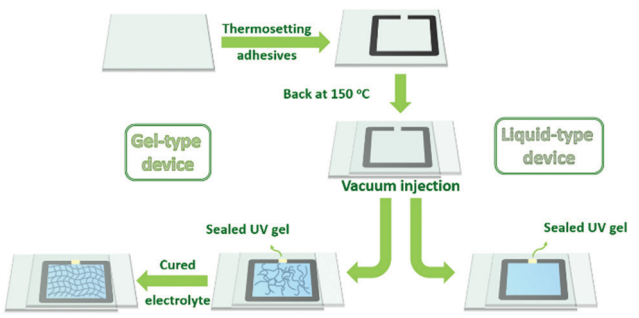

Fig. 5 A schematic diagram of the procedures used to fabricate the liquid-type and gel-type devices.

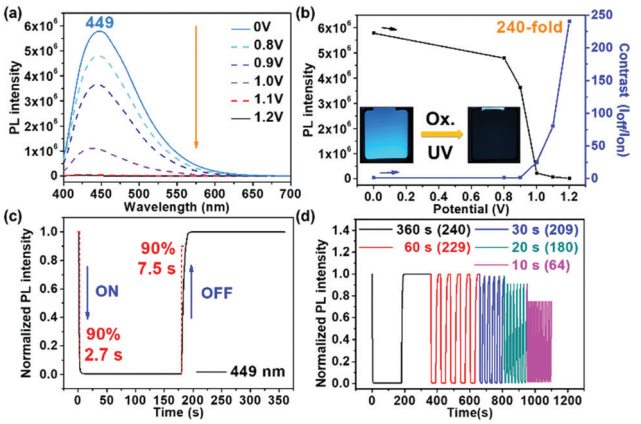

Fig. 6 (a) PL spectra, (b) potential *vs.* PL and contrast diagram, (c) fluorescence switching responses and (d) switching time test of gel type EFCDs based on **TPB/HV**. Switching time test was measured at different step cycle times of 360, 60, 30, 20 and 10 s, respectively, by applying voltage between −0.1 and 1.2 V. The devices with gap of 120 μm are derived from ITO glass with 2 cm × 2 cm active area.

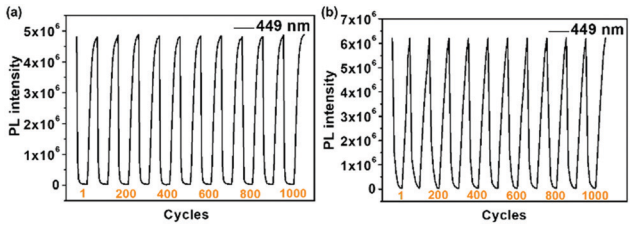

Fig. 7 Repetitive switching time test of liquid-type EFCDs based on (a) **TPPA/TPB/HV** between 1.2 V (on) and −0.1 V (off) with cycle time of 20 s, (b) **TPB/HV** between 1.2 V (on) and −0.1 V (off) with cycle time of 10 s. The devices with gap of 120 μm are derived from ITO glass with 2 cm × 2 cm active area.

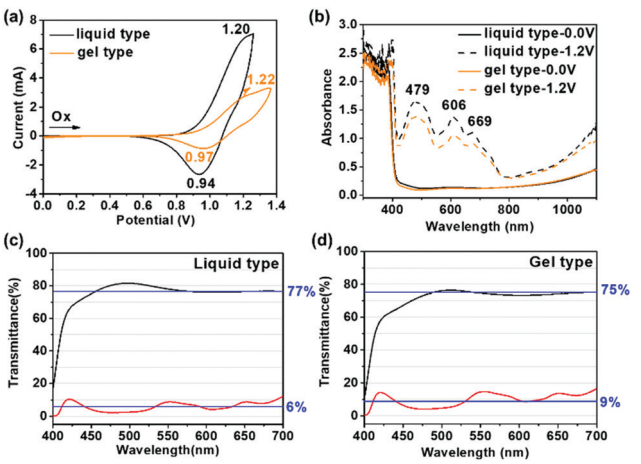

Fig. 8 (a) Cyclic voltammetric diagrams (scan rate: 50 mV s^{-1}), (b–d) absorbance and transmittance spectra (0–1.2 V) of liquid and gel-type devices based on **TPB/HV**.

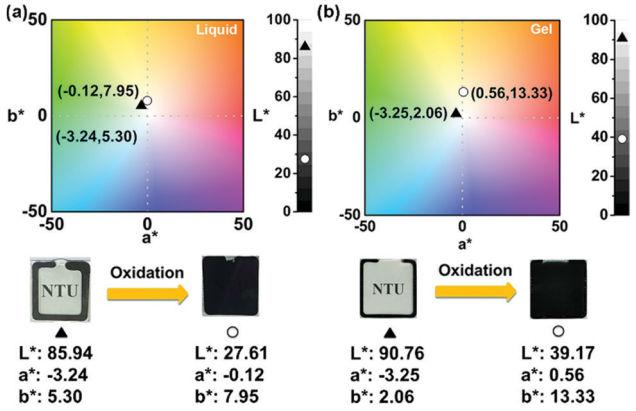

Fig. 9 CIE diagram of (a) liquid-type device and (b) gel-type device based on **TPB**/**HV**.

Fig. 8b–d. In addition, both devices displayed high transparency (L^* = 85.94 and 90.76) with low colour-opponent dimensions (a^* = −3.24 and −3.25; b^* = 5.30 and 2.06) at the original neutral form in the CIE chromaticity diagrams as shown in Fig. 9. After applying a bias of 1.2 V, the colours of both the liquid- and gel-type devices became black, caused by their low L^* values of 27.61 and 39.17, respectively. Furthermore, these highly transparent and colourless to truly black panchromatic devices also revealed very quick EC switching response capability as illustrated in Fig. S7, S8 and Table S4 (ESI†), which summarizes the EC switching response times of the different types of **TPB**/**HV** devices between 1.2 V (on) and −0.1 V (off).

Conclusions

In summary, novel all-in-one electrochemical devices that exhibited simultaneously high-performance EC and EFC behaviours were successfully prepared. The liquid-type EFCDs derived from **TPPA**/**TPB**/**HV** exhibited excellent EFC performances, including the highest PL contrast ratio (374), fast switching time, and electrochemical stability. To reduce the use of materials and fit the trend of display requirements, a gel-type device based on **TPB**/**HV** was also fabricated for comparison. The results demonstrated that both the liquid- and gel-type devices derived from the **TPB**/**HV** system showed not only extraordinary EFC characteristics but also remarkable EC performance. Furthermore, all of these devices were highly transparent and colourless in the original neutral state, and could be changed to truly black by being subjected to an oxidation process, and they could be applied as panchromatic shutters for transparent displays.

Conflicts of interest

There are no conflicts to declare.

Acknowledgements

This work was financially supported by the ''Advanced Research Center for Green Materials Science and Technology'' from The Featured Area Research Center Program within the framework of the Higher Education Sprout Project by the Ministry of Education (109L9006) and the Ministry of Science and Technology in Taiwan (MOST 109-2634-F-002-042, 107-2113-M-002-024-MY3, and 107-2221-E-002-066-MY3).

Notes and references

1 C. S. Matsumoto, K. Shinoda, H. Matsumoto, K. Seki, E. Nagasaka, T. Iwata and A. Mizota, *J. Vision*, 2014, **14**, 1–14.
2 F. M. Tseng, A. C. Cheng and Y. N. Peng, *Technol. Forecast. Soc. Change.*, 2009, **76**, 897–909.
3 D. E. Mentley, *Proc. IEEE*, 2002, **90**, 453–459.
4 E. A. Schaefer, R. Vogt, M. Brankl, M. Zeiner, M. Keller, W. Schubert, S. Warmuth, T. Kloiber, D. Blume and J. Herrmann, *US Pat.*, 20150338715, 2015.
5 J. N. Lin, C. H. Chen and C. W. Su, *US Pat.*, 20150355514, 2015.
6 P. M. Beaujuge, S. Ellinger and J. R. Reynolds, *Nat. Mater.*, 2008, **7**, 795–799.
7 G. A. Corrente, E. Fabiano, F. Manni, G. Chidichimo, G. Gigli, A. Beneduci and A. L. Capodilupo, *Chem. Mater.*, 2018, **30**, 5610–5620.
8 A. Beneduci, G. A. Corrente, E. Fabiano, V. Maltese, S. Cospito, G. Ciccarella, G. Chidichimo, G. Gigli and A. L. Capodilupo, *Chem. Commun.*, 2017, **53**, 8960–8963.
9 S. V. Vasilyeva, P. M. Beaujuge, S. J. Wang, J. E. Babiarz, V. W. Ballarotto and J. R. Reynolds, *ACS Appl. Mater. Interfaces*, 2011, **3**, 1022–1032.
10 D. Y. Liu, A. D. Chilton, P. Shi, M. R. Craig, S. D. Miles, A. L. Dyer, V. W. Ballarotto and J. R. Reynolds, *Adv. Funct. Mater.*, 2011, **21**, 4535–4542.
11 S. Hellstrom, P. Henriksson, R. Kroon, E. G. Wang and M. R. Andersson, *Org. Electron.*, 2011, **12**, 1406–1413.
12 A. L. Dyer, E. J. Thompson and J. R. Reynolds, *ACS Appl. Mater. Interfaces*, 2011, **3**, 1787–1795.
13 H. J. Yen, K. Y. Lin and G. S. Liou, *J. Mater. Chem.*, 2011, **21**, 6230–6237.
14 H. S. Liu, B. C. Pan, D. C. Huang, Y. R. Kung, C. M. Leu and G. S. Liou, *NPG Asia Mater.*, 2017, **9**, e388.
15 J. T. Wu and G. S. Liou, *Chem. Commun.*, 2018, **54**, 2619–2622.
16 J. T. Wu, H. T. Lin and G. S. Liou, *J. Mater. Chem. C*, 2018, **6**, 13345–13351.
17 C. P. Kuo, C. N. Chuang, C. L. Chang, M. K. Leung, H. Y. Lian and K. C. W. Wu, *J. Mater. Chem. C*, 2013, **1**, 2121–2130.
18 J. H. Wu and G. S. Liou, *Adv. Funct. Mater.*, 2014, **24**, 6422–6429.
19 N. Sun, K. Su, Z. Zhou, Y. Yu, X. Tian, D. Wang, X. Zhao, H. Zhou and C. Chen, *ACS Appl. Mater. Interfaces*, 2018, **10**, 16105–16112.
20 S. W. Cheng, T. Han, T. Y. Huang, B. Z. Tang and G. S. Liou, *Polym. Chem.*, 2018, **9**, 4364–4373.
21 H. J. Yen and G. S. Liou, *Prog. Polym. Sci.*, 2019, **89**, 250–287.

22 X. Zhang, Q. Lu, C. Yang, S. Zhao, Y. Chen, H. Niu, P. Zhao and W. Wang, *Eur. Polym. J.*, 2019, **112**, 291–300.
23 C. Yang, W. Cai, X. Zhang, L. Gao, Q. Lu, Y. Chen, Z. Zhang, P. Zhao, H. Niu and W. Wang, *Dyes Pigm.*, 2019, **160**, 99–108.
24 N. Sun, K. Su, Z. Zhou, X. Tian, D. Wang, N. Vilbrandt, A. Fery, F. Lissel, X. Zhao and C. Chen, *J. Mater. Chem. C*, 2019, **7**, 9308–9315.
25 Y. Kim, J. Do, E. Kim, G. Clavier, L. Galmiche and P. Audebert, *J. Electroanal. Chem.*, 2009, **632**, 201–205.
26 S. Seo, Y. Kim, Q. Zhou, G. Clavier, P. Audebert and E. Kim, *Adv. Funct. Mater.*, 2012, **22**, 3556–3561.
27 A. Beneduci, S. Cospito, M. La Deda and G. Chidichimo, *Adv. Funct. Mater.*, 2015, **25**, 1240–1247.
28 X. Wang, W. Li, W. Li, C. Gu, H. Zheng, Y. Wang, Y. Zhang, M. Li and S. X. A. Zhang, *Chem. Commun.*, 2017, **53**, 11209–11212.
29 G. A. Corrente, E. Fabiano, M. La Deda, F. Manni, G. Gigli, G. Chidichimo, A. L. Capodilupo and A. Beneduci, *ACS Appl. Mater. Interfaces*, 2019, **11**, 12202–12208.
30 J. Zhang, Z. Chen, X. Y. Wang, S. Z. Guo, Y. B. Dong, G. A. Yu, J. Yin and S. H. Liu, *Sens. Actuators, B*, 2017, **246**, 570–577.
31 H. Lim, S. Seo, S. Pascal, Q. Bellier, S. Rigaut, C. Park, H. J. Shin, O. Maury, C. Andraud and E. Kim, *Sci. Rep.*, 2016, **6**, 18867.
32 M. Higuchi, in *Intelligent Nanosystems for Energy, Information and Biological Technologies*, ed. J. Sone and S. Tsuji, Springer, Tokyo, 2016, pp. 217–248.
33 W. Gao, T. Yu, L. Wu and L. Bi, *Chem. Commun.*, 2016, **52**, 10403–10406.
34 S. Abraham, S. Mangalath, D. Sasikumar and J. Joseph, *Chem. Mater.*, 2017, **29**, 9877–9881.

